ECE540 Project II: Nonlinear Poisson FEM Iterative Solver for PN Diode

Yi-Chia Tsai (NetID: yichiat2)[a)]
Department of Electrical and Computer Engineering, University of Illinois at Urbana-Champaign, Urbana, Illinois 61801, USA and Micro and Nanotechnology Laboratory, University of Illinois at Urbana-Champaign, Urbana, Illinois 61801, USA

(Dated: 14 November 2019)

Finite–Element Method (FEM) has been implemented to solve nonlinear Poisson equations for the potential profile of PN diode, where Newton–Raphson method has been implemented to update each matrix element iteratively. To improve the accuracy and convergence at the junction region, non-uniform meshes are generated on the direction normal to the junction. As the results, the potential profile in PN junction at equilibrium condition is consistent with analytical solutions derived under depletion approximations and even goes beyond and recover correct physics at the edges of the junction. The objectives of this project are to understand how to decompose a large simulation domain into several individual elements, assemble the elements into an interacting matrix, and solve the matrix iteratively for a wide range of engineering applications.

Keywords: Nonlinear Poisson Equations, Finite–Element Method, Newton-Raphson Method, PN Diode, Device Physics

I. INTRODUCTION

In the semiconductor area, PN diode is the fundamental device that has been widely used in photodetectors, photovoltaic cells, light-emitting diodes, and rectifiers. By connecting two PN diodes with opposite direction, a transistor is built, which is the fundamental component in logic circuits, RF circuits, and amplifiers. It is safe to say that PN diodes are the building block to construct the modern civilization. Both diodes and transistors are functioned by manipulating the potential profile in the devices, which cannot be measured directly through experiments. Therefore, it is an important task to investigate the potential profile using existent theory solved by numerical approach.

Potential distribution can be modeled by Poisson equation, which states that the Laplacian of potential is equal to the charges divided by the material dielectric constant. It is plausible to solve the Poisson equation in one–dimensional case analytically with a fixed point–charge. The result degenerates into the Coulomb potential produced by a point–charge. However, several difficulties prohibit engineers from solving Poisson equation in PN diodes without making certain approximations[1]. First of all, the P-type and N-type semiconductors in PN diodes are fabricated asymmetrically, which implies the necessity of two-dimensional simulation. Second, the charges contribute from multiple sources, including electrons, holes, ionized donors, and ionized acceptors, which are non-uniformly distributed in the junction region. Third, the electron and hole concentrations are exponentially dependent on the potential, resulting in nonlinear Poisson equation as shown in Eq. (1),

$$\begin{aligned} -\nabla \cdot (\varepsilon \nabla \phi) &= q\left(p - n + N_D - N_A\right) \\ &= q\left(n_i e^{(-\frac{\phi}{V_T})} - n_i e^{(\frac{\phi}{V_T})} + N_D - N_A\right) \end{aligned} \tag{1}$$

where $q = 1.602 \times 10^{-19}\ C$, $\varepsilon = 11.7\ \varepsilon_0$, $V_T = 25.9\ mV$, p, n, $n_i = 1.5 \times 10^{10}\ cm^{-3}$, N_D, and N_A are elementary charge constant, material dielectric constant, thermal potential, hole concentration, electron concentration, intrinsic carrier concentration, donor concentration, and acceptor concentration, respectively. As a consequence, solving the nonlinear Poisson equation in 2D requires numerical discretization, where the solution has to be obtained by iterative algorithm due to the potential-dependent charges.

In this project, finite-element method (FEM)[2], inherent from Galerkin's method, is applied to discretize the PN diode into multiple elements, where the non-uniform meshes are generated manually to improve the accuracy and convergence at the narrow junction area, which is typically at scale of $\approx 0.5\ \mu m$. For the iterative method, Successive Over-Relaxation (SOR) fails to reach convergence due to the exponential sensitivity of electron and hole concentration on potential, which explodes the equation with astronomically colossal charges after the first iteration. To take the sensitivity into account, Newton–Raphson method[3] expressed the sensitivity with Jacobian matrix is applied to solve the discretized potential iteratively.

II. COMPUTATIONAL MODEL AND DEVICE STRUCTURE

A. Finite–Element Formulation

The Eq. (1) is reformulated by normalizing the potential ϕ with respect to V_T as shown in Eq. (2), where the

[a)]Address: Innovative COmpound semiconductoR (ICOR) Laboratory, Urbana, Illinois 61801, USA. Electronic mail: yichiat2@illinois.edu. Telephone: +1 (217) 974-5750. URL: `http://icorlab.ece.illinois.edu`.

normalized potential $\psi = \frac{\phi}{V_T}$. Once the target equation is defined, the weighting function is applied on the both sides of Eq. (2) with double inetegral across the entire simulation domain. Notably, the choose of weighting function is identical to the potential interpolation function (N_i) known as Galerkin's method as formulated in Eq. (3).

$$-\nabla \cdot (\varepsilon \nabla \psi) = \frac{q}{V_T}\left(n_i e^{-\psi} - n_i e^{\psi} + N_D - N_A\right), \tag{2}$$

$$\begin{aligned} &-\iint_{\mathbf{S}} N_i \nabla \cdot (\varepsilon \nabla \psi)\, d\mathbf{S} \\ &\quad = \iint_{\mathbf{S}} \frac{q}{V_T} N_i \left(n_i e^{-\psi} - n_i e^{\psi} + N_D - N_A\right) d\mathbf{S} \end{aligned} \tag{3}$$

The left-hand side can be simplified by using vector identity and assuming Neumann boundary condition shown as

$$-\iint_{\mathbf{S}} N_i \nabla \cdot (\varepsilon \nabla \psi)\, d\mathbf{S} = \iint_{\mathbf{S}} \varepsilon \nabla N_i \cdot \nabla \psi d\mathbf{S}. \tag{4}$$

Notably, the spirit of FEM is to express the potential at arbitrary positions as a linear combination of basis functions, which are the target potentials that are going to be solved later on. Hence, the potential at arbitrary positions is formulated by

$$\psi = \sum_{j=1}^{N} N_j \psi_j, \tag{5}$$

where N, N_j, and ψ_j are the total number of nodes, the interpolation at node j, and the potential at node j,respectively. By combining Eqs. (3) to (5), the Eq. (2) can be formulated by interpolation functions and discretized potentials as shown in Eq. (6). Since index i ranges from 1 to N, therefore, it is worth noting that solving Eq. (6) is equivalent to solve a matrix problem: $[\mathrm{K}]_{N\times N}[\psi]_{N\times 1} = [\mathrm{b}(\psi)]_{N\times 1}$. Given the localized nature of interpolation functions, the matrix element in Eq. (6) can be constructed by the superposition of individual elements as formulated in Eq. (7). M is the total number of elements. l, m, and n are the three indices of each element e. The major difference between Eq. (6) and Eq. (7) is that Eq. (6) constructs the matrix row by row; whereas, Eq. (7) constructs the matrix element by element, i.e. block by block. For instance, for each element, the left-hand side of Eq. (7) generates a 3-by-3 matrix; while the right-hand side generates a 3-by-1 matrix. The first (hole contribution) and second (electron contribution) double integrals on the right-hand side are evaluated numerically by mapping onto shape functions.

$$\sum_{j=1}^{N} \psi_j \iint_{\mathbf{S}} \varepsilon \nabla N_i \cdot \nabla N_j d\mathbf{S} = \frac{q n_i}{V_T}\left(\iint_{\mathbf{S}} N_i e^{-\sum_{j=1}^{N} N_j \psi_j} + \iint_{\mathbf{S}} N_i e^{\sum_{j=1}^{N} N_j \psi_j}\right) d\mathbf{S} + \frac{q\left(N_D - N_A\right)}{V_T} \iint_{\mathbf{S}} N_i d\mathbf{S} \tag{6}$$

$$\begin{aligned} \sum_{e=1}^{M} \psi_m \iint_{\mathbf{S}^e} \varepsilon \nabla N_l^e \cdot \nabla N_m^e d\mathbf{S}^e &= \sum_{e=1}^{M} \frac{q n_i}{V_T} \iint_{\mathbf{S}^e} N_l^e e^{-N_l^e \psi_l - N_m^e \psi_m - N_n^e \psi_n} d\mathbf{S}^e \\ &+ \sum_{e=1}^{M} \frac{q n_i}{V_T} \iint_{\mathbf{S}^e} N_l^e e^{N_l^e \psi_l + N_m^e \psi_m + N_n^e \psi_n} d\mathbf{S}^e + \sum_{e=1}^{M} \frac{q\left(N_D - N_A\right)}{V_T} \iint_{\mathbf{S}^e} N_i^e d\mathbf{S}^e \end{aligned} \tag{7}$$

B. Newton–Raphson Iteration

Once the matrices: $[\mathrm{K}]_{N\times N}[\psi]_{N\times 1} = [\mathrm{b}(\psi)]_{N\times 1}$ are constructed, $[\psi]$ has to be solved iteratively. An intuitive approach is set initial guess of $[\psi^0]$ and solve $[\psi^{k+1}] = [\mathrm{K}]^{-1}[\mathrm{b}(\psi^k)]$ until $|\psi^{k+1} - \psi^k|$ is smaller than tolerance. However, this approach leads to divergence because of the exponential sensitivity of [b] on ψ. A few percent overestimation on $[\psi^{k+1}]$ leads to astronomically large [b] in the next iteration. Therefore, Newton-Raphson method is used to update $[\psi^{k+1}]$ by taking the exponential sensitivity into account.

Newton-Raphson method originates from the linear approximation of N-dimensional multivariate functions in Tylor expansion:

$$f_i(\mathbf{x} + \delta\mathbf{x}) \approx f_i(\mathbf{x}) + \sum_{j=1}^{N} \frac{\partial f_i(\mathbf{x})}{\partial x_j} \delta x_j \quad (i = 1...N), \tag{8}$$

which can be formulated in a matrix form:

$$\begin{aligned}\mathbf{f}(\mathbf{x}+\delta\mathbf{x}) &= \mathbf{f}(\mathbf{x}) + \begin{bmatrix} \frac{\partial f_1}{\partial x_1} & \cdots & \frac{\partial f_1}{\partial x_N} \\ \vdots & \ddots & \vdots \\ \frac{\partial f_N}{\partial x_1} & \cdots & \frac{\partial f_N}{\partial x_N} \end{bmatrix} \begin{bmatrix} \delta x_1 \\ \vdots \\ \delta x_N \end{bmatrix} \\ &= \mathbf{f}(\mathbf{x}) + \mathbf{J}(\mathbf{x})\delta\mathbf{x},\end{aligned} \tag{9}$$

where $\mathbf{f}(\mathbf{x}+\delta\mathbf{x}) = 0$ if appropriate correction terms ($\delta\mathbf{x}$) are found, which can be calculated by Jacobian matrix ($\mathbf{J}$). As a result, the updated x^{k+1} can be expressed as

$$\begin{aligned}\mathbf{x}^{k+1} &= \mathbf{x}^k + \delta\mathbf{x} \\ &= \mathbf{x}^k - \mathbf{J}^{-1}(\mathbf{x}^k)\mathbf{f}(\mathbf{x}^k)\end{aligned} \tag{10}$$

In my FEM formulation, the matrix $\mathbf{f}$ in Eq. (10) is equivalent to [K][ψ] - [b(ψ)] in Eq. (7), whereas the vector $\mathbf{x}$ is equivalent to the vector ψ. However, an additional effort of calculating Jacobian matrix under FEM formalism has to be paid in order to take the information of exponential sensitivity into account. The Jacobian matrix element can be obtained by partial derivative Eq. (6) with respect to each nodal potential (ψ) as formulated in Eq. (11). It is worth noting that Eq. (11) calculates the individual matrix element (i,j) , unlike Eq. (6), which calculates a row of elements.

$$\frac{\partial \mathbf{f}_i}{\partial \psi_j} = \iint_{\mathbf{S}} \varepsilon \nabla N_i \cdot \nabla N_j d\mathbf{S} + \frac{qn_i}{V_T}\left(\iint_{\mathbf{S}} N_i N_j e^{-\sum_{k=1}^{N} N_k \psi_k} + \iint_{\mathbf{S}} N_i N_j e^{\sum_{k=1}^{N} N_k \psi_k}\right) d\mathbf{S} \tag{11}$$

$$\begin{aligned}\mathbf{J}(\psi) = &\sum_{e=1}^{M} \iint_{\mathbf{S}^e} \varepsilon \nabla N_l^e \cdot \nabla N_m^e d\mathbf{S}^e + \sum_{e=1}^{M} \frac{qn_i}{V_T} \iint_{\mathbf{S}^e} N_l^e N_m^e e^{-N_l^e\psi_l - N_m^e\psi_m - N_n^e\psi_n} d\mathbf{S}^e \\ &+ \sum_{e=1}^{M} \frac{qn_i}{V_T} \iint_{\mathbf{S}^e} N_l^e N_m^e e^{N_l^e\psi_l + N_m^e\psi_m + N_n^e\psi_n} d\mathbf{S}^e\end{aligned} \tag{12}$$

Similarly, using the localized nature of interpolation functions, Eq. (11) can be decomposed into elements and calculated by superposition from the elements. As a result, the Jacobian matrix can be constructed element by element as shown in Eq. (12). For each element, the three double integrals in Eq. (12) construct a 3-by-3 matrix contributing to 9 matrix elements in $\mathbf{J}$. Once the Jacobian matrix is constructed, $\mathbf{x}^k = [\psi^k]$, $\mathbf{f}(\mathbf{x}^k) = [K][\psi^k] - [b(\psi^k)]$, and $\mathbf{J}$ are input into Eq. (10) to solve for $[\psi^{k+1}]$ iteratively until $|\psi^{k+1} - \psi^k| < 10^{-6}$.

C. Device Geometry and Boundary Conditions

The geometry of PN diode is define in Fig. 1. The width and height are set as 2 μm, where the height of each type is 1 μm. According to device physics, when N-type semiconductor is in contact with P-type semiconductor, the electrons in N-type and the holes in P-type diffuse from one side to the other due to Brownian motion and concentration gradient. As a result, a junction forms at the contact region, which alters the potential at the junction to reflect the diffusion of electron and hole concentrations. Since the doping concentrations on both types are assumed to be symmetric ($N_D = N_A = 10^{16}\ cm^{-3}$), the junction width on N-type and P-type semiconductors is expected to be symmetric as well.

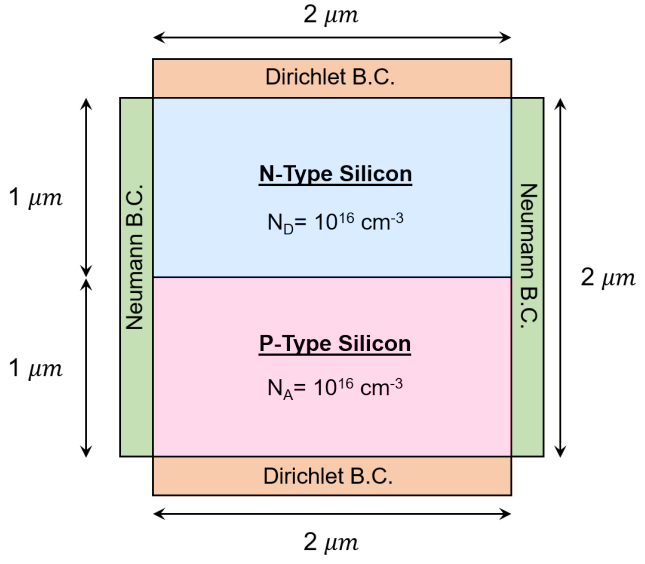

FIG. 1 Schematic illustration and doping concentration of the PN diode.

In Fig. 1, Neumann boundary conditions are applied on the edges of the PN diode. Because the FEM discretiza-

tion in Eq. (7) already considers the Neumann boundary condition automatically, no additional treatment has to be done during the matrix constructions. On the other hand, two different Dirichlet boundary conditions are applied on N-type and P-type semiconductor separately. In device physics, Dirichlet boundary conditions are given by external bias. Since this project focuses on the potential profile at equilibrium, where there is no current flows inside the PN diode. Zero bias is applied on N-type and P-type semiconductors. Therefore, the potentials at Dirichlet boundaries should obey charge neutrality condition ($p-n+N_D-N_A=0$) and mass action law ($np=n_i^2$). As a result, the potentials at Dirichlet boundaries can be expressed as

$$\psi_D = \ln\left(\frac{N_D - N_A}{2n_i} + \sqrt{\frac{(N_D - N_A)^2}{4n_i^2} + 1}\right). \tag{13}$$

This implies that the potentials is positive in the N-type region and is negative in the P-type region.

D. Non-Uniform Mesh Generation

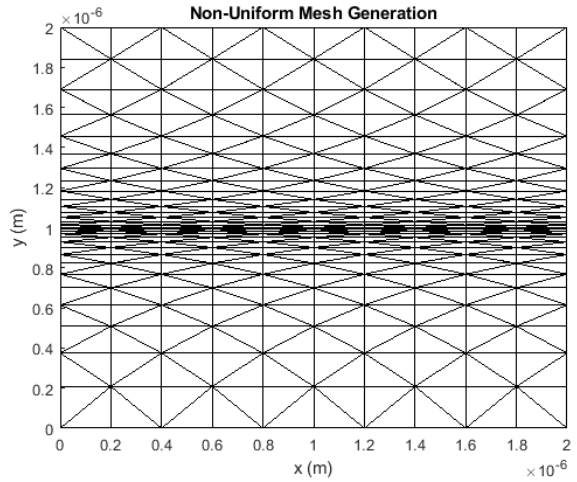

FIG. 2 Non-uniform mesh generated on the y direction in order to increase the simulation resolution at the junction region.

Figure 2 demonstrates the mesh generation on the device structure depicted in Fig. 1. 11 uniform nodes are sampled on the x axis, which leads to 10 elements on the x axis. On the other hand, 31 non-uniform nodes are sampled on the y axis, which results in 30 elements on the y axis. The non-uniform mesh on the y axis is generated through geometric progression. For example, if N nodes are sampled in [0, 1] region, the axis of individual node can be defined as follow

$$\begin{aligned} &y(1) = 0 \\ &y(2) = h \\ &y(3) = h + r \cdot h \\ &\vdots \\ &y(N) = h + r \cdot h + r^2 \cdot h + \cdots + r^{N-2} \cdot h = 1, \end{aligned} \tag{14}$$

where r is the ratio to manipulate the mesh distribution. $r < 1$ means that the meshes become denser as it approaches the end; whereas, $r > 1$ implies that the meshes are dense in the beginning and become sparser in the end. $r = 1$ leads to an uniform mesh. h can be calculated by geometric sum:

$$h = \frac{r-1}{r^{N-1}-1}. \tag{15}$$

Therefore, in order to have dense meshes at the center region, the meshes are generated separately in P-type and N-type regions. In the P-type region, $r = 0.8$ is given; while, $r = 1.2$ is applied in the N-type region. After the nodes are sampled non-uniformly, the y coordinates in P-type and N-type regions are assigned by multiplying Eq. (14) with the size, i.e. height, of each region to extend the domain of Eq. (14) from [0, 1] to [0, 1 μm]. Finally, two sets of meshes are combined, which results in Fig. 2. It is worth mentioning that, after the grids are defined, each element with corresponding three indices is labeled and stored into an M-by-3 array accomplished by a nested for–loop, i.e. the mesh generator is implemented by the author.

III. RESULTS AND DISCUSSION

Although the FEM simulation is developed for 2D case, given the symmetry of PN diode in Fig. 1, the simulation results can be sliced into 1D case for clearer comparisons.

A. Discretization Error Analysis

The dependence of potential on mesh generation can be boiled down into the contributions from mesh density and mesh distribution.

1. Mesh Density

Given the steep potential change in the junction region, the mesh discretization across the junction region predominantly impacts the accuracy of potential distribution and, especially, charge concentration due to the exponential dependence of charge on the potential. Fig. 3 shows the potential profile across the junction region at $x = 0.8\ \mu m$ for different numbers of elements generated

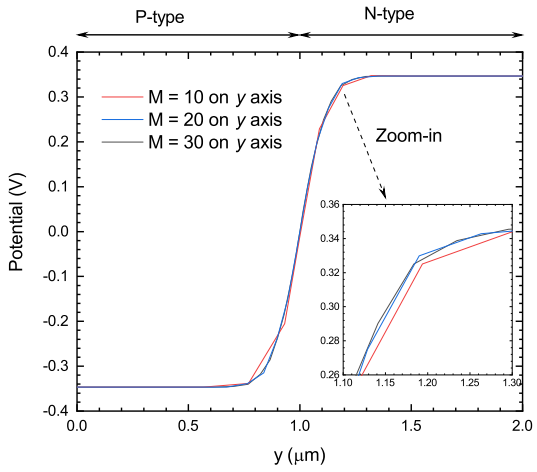

FIG. 3 Potential as a function of y for different mesh number on the y axis, where $x = 0.8\ \mu m$.

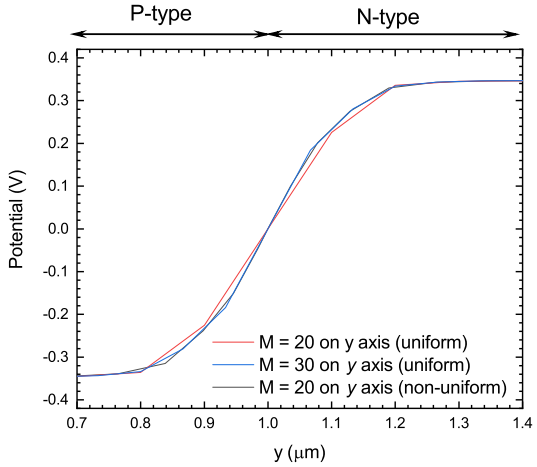

FIG. 4 Potential as a function of y for different mesh number and uniformity on the y axis, where $x = 0.8\ \mu m$.

on the y direction. In the simulations, 10, 20, and 30 elements are generated on the y direction for each x grid. Since there are 11 x-grid points, 200 ("M = 10 on y axis"), 400 ("M = 10 on y axis"), and 600 ("M = 10 on y axis") elements generated in the entire simulation domain, where the [K] matrix size in Eq. (7) is $14,641$, $53,361$, and $116,281$, respectively. The denser elements at the junction region leads to the higher the accuracy. However, according to the expansion of [K] matrix, the computational effort increases quadratically with respect to the elements on the y axis. In the zoom-in plot of Fig. 3, "M = 10 on y axis" cannot reproduce the steep changes in the junction region and underestimates the potential by 1.5% imposing an further underestimation of 17.5% on electron concentration. On the other hand, "M = 20 on y axis" and "M = 30 on y axis" show infinitesimal discrepancy even in the steep junction region, implying that the resolution is reached if the number of elements on the y direction is larger than 20. The achievement of high resolution with small matrix size is ascribed to the implementation of non-uniform mesh on the y direction.

2. Uniform v.s. Non-Uniform Mesh

To demonstrate the importance of non-uniform mesh on the accuracy of potential at the junction region, Fig. 4 shows the potential distribution as a function of y for different mesh number and uniformity on the y axis, where $x = 0.8\ \mu m$. First of all, the red and black lines have the same meshes and [K] matrix size, but the former is calculated with uniform mesh; while, the latter uses non-uniform mesh as described in Section II D. It can be seen that the uniform mesh underestimates the potential by more than 14%, resulting in an underestimation of 60.8% on the electron concentration, which is even worse than the 17.5% using "M = 10 on y axis" with non-uniform mesh as illustrated in Fig. 3 and discussed in Section III A 1. Therefore, the number of elements should be increased in the uniform case in order to reproduce the same accuracy achieved using the non-uniform mesh. As shown in the blue line, which has 600 elements and a matrix size of $116,281$, the accuracy is eventually comparable with the black line (non-uniform mesh), which uses only 400 elements and a matrix size of $53,361$ (twice computational and storage efficiency). This result shows that implementing non-uniform mesh is necessary to achieve higher accuracy with lower computational and storage costs. In short, by combining the conclusion made after mesh density analysis (Section III A 1) and mesh distribution analysis, the "M = 30 on y axis" non-uniform mesh is generated for further discussion.

B. Comparison with Analytical Solutions

$$\phi = \begin{cases} 0, & \text{if } y < y_c - y_p \\ \frac{qN_A}{2\varepsilon_s}\left[(y-y_c)+y_p\right]^2, & \text{if } y_c - y_p < y < y_c \\ \frac{qN_A y_p^2}{2\varepsilon_s} + \frac{qN_D}{2\varepsilon_s}(y-y_c)(2y_n - y + y_c), & \text{if } y_c < y < y_c + y_n \\ \frac{qN_A y_p^2}{2\varepsilon_s} + \frac{qN_D y_n^2}{2\varepsilon_s}, & \text{if } y > y_c + y_n \end{cases} \tag{16}$$

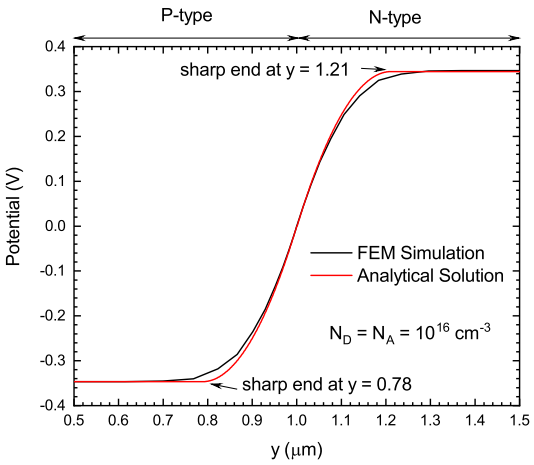

FIG. 5 Comparison of Potential distribution at the junction with a symmetric doping of $N_D = N_A = 10^{16}\ cm^{-3}$ between FEM simulation and analytical solution, where $x = 0.8\ \mu m$.

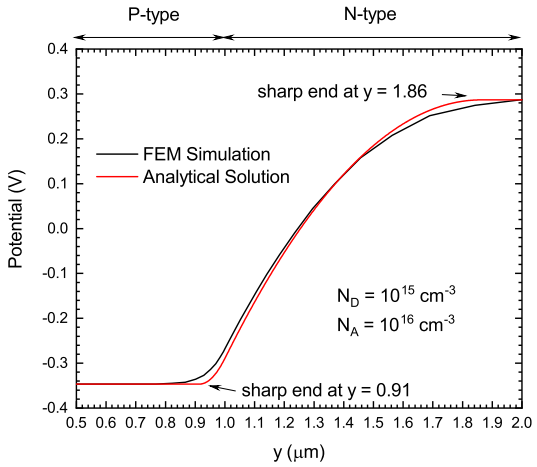

FIG. 6 Comparison of Potential distribution at the junction with an asymmetric doping ($N_D = 10^{15}\ cm^{-3}$ and $N_A = 10^{16}\ cm^{-3}$) between FEM simulation and analytical solution, where $x = 0.8\ \mu m$.

Given the complexity of nonlinear Poisson equation, certain idealizations are imposed to derive the analytical solution of potential in the PN diode. First of all, the depletion approximation assumes that the electron and hole concentrations are zero inside the junction region. As a result, the charges in the junction region are contributed by the ionized donors (N_D on the N-side junction) and acceptors (N_A on the P-side junction). Second, the regions outside of the junction is charge neutral, implying constant potential. Third, the device has a perfect symmetry with infinitely large width so that the potential only depends on the direction normal to the junction. Under these assumptions, the potential can be calculated analytically as a function of y (the direction normal to the junction) as derived in Eq. (16), where y_c, y_n, and y_p are the center of junction and the depletion width in the N-type and P-type regions, respectively. Notably, y_c, y_n, and y_p can be calculated analytically based on the coordinate of the junction and the doping concentrations as formulated in Eq. (17).

Fig. 5 compares the FEM simulation with the analytical solution (Eq. (16)) for a symmetric doping condition of $N_D = N_A = 10^{16}\ cm^{-3}$. It can be seen that the potential distribution calculated under FEM formalism is extremely accurate at the center of the junction, this is because the assumption of depletion approximation is especially valid at the center of the junction. In the junction region, the positively-charged ionized donors and negatively-charged acceptors create an built-in electric field, repelling electrons and holes further away from the junction region. The built-in electric field reaches its maximum at the center of the junction, therefore, the electron and hole concentrations at the center of the junction are infinitesimally small, which can be ignored compared to the ionized donor and acceptor concentrations. On the contrary, a discrepancy is observed between the FEM simulation and the analytical solution at the edges of the junction because the electron and hole concentrations cannot be ignored as the built-in electric field is weak compared to the center of the junction. Consequently, the depletion approximation fails to depict the potential distribution at the edges of the junction, i.e. the analytical solution underestimates the depletion width; whereas, the FEM simulation is able to retrieve the true physics of PN diode.

One of the important features of PN diode is that the depletion width and the potential can be manipulated by doping concentration. In order to test the generality of the FEM algorithm, Fig. 6 demonstrates the potential distribution with an asymmetric doping concentration of $N_D = 10^{15}\ cm^{-3}$ and $N_A = 10^{16}\ cm^{-3}$. Similarly, the FEM solution expects a wider depletion width than the analytical solution since the depletion approximation is inaccurate at the edges of the junction. Within the expectation, the depletion width on the P-side is narrower than the N-side because the ionized donor concentration on the N-side is an order magnitude smaller than the ionized acceptor concentration on the P-side, hence, a wider depletion width on the N-side is required to satisfy the charge neutrality condition at the junction region. In short, Figs. 5 and 6 have reflected several advantages of FEM simulation over analytical solutions and proven the necessity of FEM algorithm beyond analytical solutions in learning PN diode.

$$\begin{cases} y_n = \sqrt{\frac{2\varepsilon_s V_T}{q}\ln(\frac{N_A N_D}{ni^2})\frac{N_A}{N_D(N_A+N_D)}} \\ y_p = \sqrt{\frac{2\varepsilon_s V_T}{q}\ln(\frac{N_A N_D}{ni^2})\frac{N_D}{N_A(N_A+N_D)}} \\ y_c = 1\ \mu m \end{cases} \tag{17}$$

C. Convergence Analysis

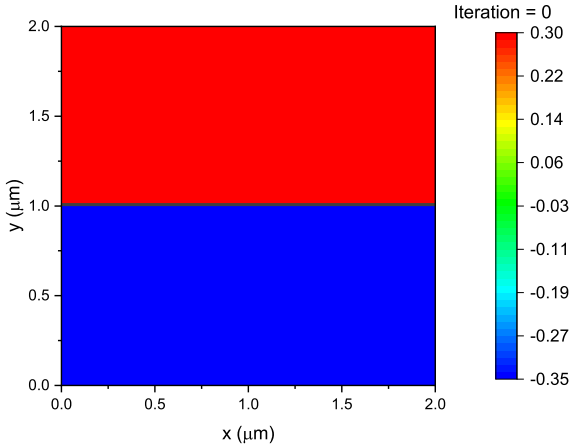

FIG. 7 The initial guess of potential for the PN diode with the asymmetric doping concentration of $N_D = 10^{15}\ cm^{-3}$ and $N_A = 10^{16}\ cm^{-3}$.

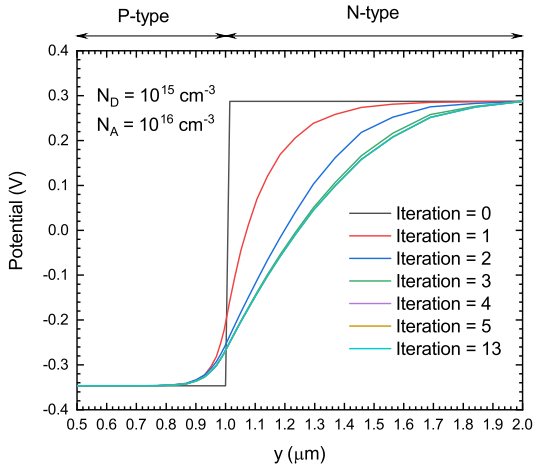

FIG. 8 Potential as a function of y for the initial guess, the first five iterations, and the final iteration, where $x = 0.8\ \mu m$.

The convergence of solutions is one of the important aspect to demonstrate the applicability of this project for more advanced engineering problems. Therefore, an efficient iterative algorithm should be used. Newton-Raphson algorithm features quadratic convergence if the first derivative of the functions is exist and the initial guess is close to the exact solution[3]. In the Poisson equation, the first derivative exists and has been derived in Eq. (11). The main concern is to generate a set of initial guess. Fortunately, the device physics and analytical solutions provide an intuitive starting point for generating initial value. According to the device physics, the potentials in the PN diode are within the range imposed

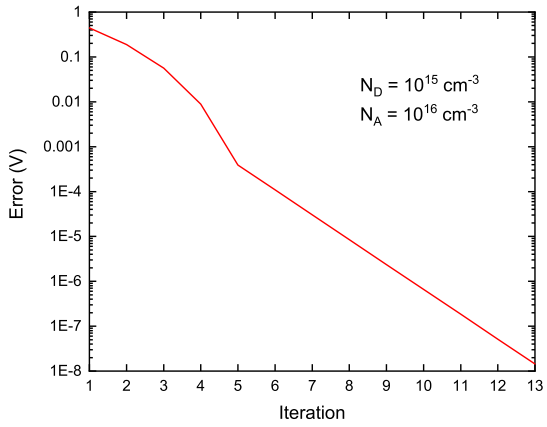

FIG. 9 Error as a function of iterations.

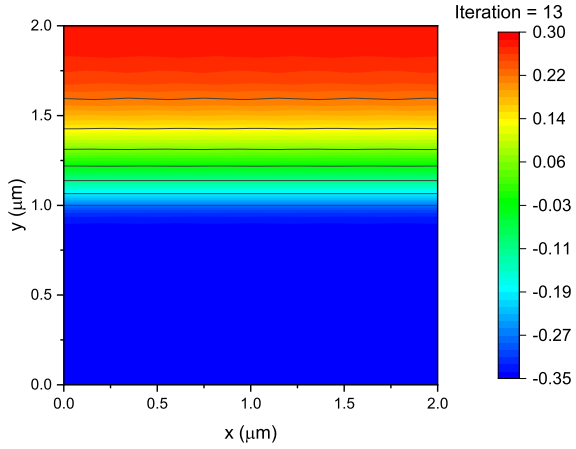

FIG. 10 The converged potential of the PN diode with the asymmetric doping concentration of $N_D = 10^{15}\ cm^{-3}$ and $N_A = 10^{16}\ cm^{-3}$.

by Dirichlet boundary conditions. For example, if the Dirichlet boundary condition on N-type and P-type regions are $\phi = 3.0V$ and $\phi = -3.5V$, respectively. The potential of arbitrary positions in PN diode is within [-3.5V, 3.0V]. Also, the junction region is narrow compared to the entire simulation domain. Therefore, its safe to guess the potentials in the entire N-type region to be same as the N-side Dirichlet boundary condition. Likewise, the potentials in the entire P-type region are guessed using the P-side Dirichlet boundary condition. Using the PN diode with the asymmetric doping concentration of $N_D = 10^{15}\ cm^{-3}$ and $N_A = 10^{16}\ cm^{-3}$ (the same condition applied in Fig. 6) as an example, Fig. 7 shows the initial guess of potential in the entire PN diode. Due to the symmetricity of the PN diode, it is more straightforward to analyze the evolution of potential for each iteration in 1D. Therefore, Fig. 8 plots the potential distribution for the initial guess, the first five iterations,

and the final iteration, where $x = 0.8\ \mu m$. It can be seen that the potential at the junction region undergoes significant changes in the first 3 iterations because the initial guess is not close enough to the exact solution. However, the initial guess still gives a reasonable value, thus the iteration does not diverge in the beginning. After 5 iterations, the difference is negligible and reaches convergence at the thirteenth iteration where $\Delta\psi < 10^{-6}$, i.e. $\Delta\phi < 3 \times 10^{-8}$ V. Fig. 9 plots the error as a function of iterations. The error is smaller than 1 meV after the first 5 iterations, which means that the deviation of electron concentration is smaller than 4%. On the other hand, the linear relationship between error and iteration in the log-scale implies the quadratic convergence of Newton-Raphson method. After 13 iterations, the error reaches 3×10^{-8} V, implying 1 ppm accuracy in the electron concentration. Finally, Fig. 10 shows the potential profile of the entire PN diode after convergence.

IV. CONCLUSIONS

In conclusion, the nonlinear Poisson FEM solver has been implemented using Newton-Raphson iteration method and has been used to study the potential profile of PN diode at equilibrium condition. The discretization error can be improved by either increasing the number of elements or using non-uniform mesh. I found that using non-uniform mesh can achieve the same discretization accuracy with twice faster computational speed and half memory usage. The FEM simulation is inconsistent with analytical solution at the center of the junction due to the validity of depletion approximation. Interestingly, the FEM simulation has been found to reflect the correct physics at the edges of the junction, which cannot be described accurately by the analytical solution. Therefore, investigating device physics necessitates FEM simulation. Finally, the quadratic convergence of Newton-Raphson method has been captured and proven to reach high accuracy in potential and charge concentrations.

ACKNOWLEDGEMENT

This work is supported by the National Science Foundation Faculty Early Career Development (CAREER) Program under award number NSF-ECCS-16-52871. The authors acknowledge the computational resources allocated by Extreme Science and Engineering Discovery Environment (XSEDE) with No. TG-DMR180050 and TG-DMR180075.

[1] "p-n junctions," in *Physics of Semiconductor Devices* (John Wiley & Sons, Ltd, 2006) pp. 77–133, https://onlinelibrary.wiley.com/doi/pdf/10.1002/9780470068328.ch2.

[2] H. Kobeissi, F. M. Ghannouchi, and A. Khebir, Journal of Applied Physics **74**, 6186 (1993).

[3] C. T. Kelley, *Solving Nonlinear Equations with Newton's Method* (Society for Industrial and Applied Mathematics, 2003) https://epubs.siam.org/doi/pdf/10.1137/1.9780898718898.

Appendix A: Source Code Implemented in MATLAB R2019a